J Nanostruct 13(3): 729-746, Summer 2023

RESEARCH PAPER

Co(II) Removal from Aqueous Solution by Birhodanine-Functionalized Magnetite Nanoparticles: Kinetic and Thermodynamic Studies

Arman Rahmaninia [1,2], Yagoub Mansoori [1,3], Farough Nasiri [1]*

[1] Department of Applied Chemistry, Faculty of Science, University of Mohaghegh Ardabili, Ardabil, Iran

[2] Nanotechnology Department, Faculty of Engineering, University of Guilan, Rasht, Iran

[3] Nanoscience and Nanotechnology Research Group, University of Mohaghegh Ardabili, Ardabil, Iran

ARTICLE INFO

Article History:
Received 04 March 2023
Accepted 19 May 2023
Published 01 July 2023

Keywords:
Adsorption
Birhodanine
Co(II) Removal
Magnetic Nanoparticles
Silylation

ABSTRACT

The present work explains the synthesis of [(E)-5-(3-(3-(trimethoxysilyl)propyl)-4-oxo-2-thioxothiazolidin-5-ylidene)-3-phenethyl-2-thioxothiazolidin-4-one] (TMOS-BIRD) to silylate magnetite nanoparticles (MNPs), and removal of Co(II) ions. The prepared NPs were characterized by FTIR analysis, scanning electron microscopy (SEM), transmission electron microscopy (TEM), X-ray diffraction (XRD), and vibrating sample magnetometry (VSM). Based on thermogravimetric analysis (TGA), the birhodanine content of the prepared nano-particles (NPs) was obtained as 48 mg g^{-1}. The capability of MNP@BIRD for removal of Co(II) cations was shown investigated under the optimal conditions of contact time, pH, adsorbent dosage and initial Co(II) concentration. The results declared that the adsorption kinetics obeys pseudo-first-order kinetics while fitting of the adsorption data into the Langmuir isotherm outlined the maximum adsorption capacity of 6.02 mg g^{-1}. The value was in accordance the experimental value ($Q_{e.exp}$ = 5.36 mg g^{-1}). Thermodynamic investigations unraveled the spontaneous nature of the adsorption process (ΔG = -5.37 kJ mol^{-1}, at 25±1°C). The positive ΔH and ΔS values (ΔH = 30.81 kJ mol^{-1}, ΔS = 123.55 J $mol^{-1}.K^{-1}$) revealed the endothermic nature of the adsorption process while randomness at the solid/liquid interface is increased during. In addition, the MNP@BIRD Nps were regenerated by simple washing with an aqueous 0.1 M HCl solution. The study of the reusability of the prepared magnetic sorbent revealed that MNP@BIRD NPs can be reused several times without any significant decrease in its extraction efficiency. These findings suggest that the silylated NPs are stable and reusable, and they can be applied to removal of Co(II) cations in water treatment processes.

How to cite this article
Rahmaninia A, Mansoori Y, Nasiri F.. Co(II) Removal from Aqueous Solution by Birhodanine-Functionalized Magnetite Nanoparticles: Kinetic and Thermodynamic Studies. J Nanostruct, 2023; 13(3):729-746. DOI: 10.22052/JNS.2023.03.014

INTRODUCTION

Although trace concentrations of certain heavy metals are metabolically needed, their unnecessary dosages may have serious side effects on critical organs such as brain, kidney, heart, liver, etc. [1, 2]. One of the trace metals in biological

* Corresponding Author Email: ya_mansoori@uma.ac.ir

systems is cobalt. Apart from cyanocobalamin, the only known cobalt function, high levels of other cobalt resources are environmentally and biologically toxic [3, 4]. Cyanocobalamin is the metal component of vitamin B1. The genotoxic effect and oxidative DNA damaging of cobalt metal and its salts are distinguished. It is believed that Co(II) competes with Ca(II) for intracellular M(II) binding proteins and prevents Ca(II) entry. Moreover, cobalt can aggregate in the liver, kidney, pancreas, heart and reach a relatively high level in the skeleton and skeletal muscles [5]. Also, IARC (The International Agency for Research on Cancer) has classified cobalt as a possible human carcinogen [6].

As reported in the guidelines of WHO (World Health Organization) and EPA (Environmental Protection agency), among all employed methods for removing heavy metal ions, solid-phase extraction (SPE) has been preferred for treating water and wastewater from the environmental and economic points of view [7-12]. Simplicity, flexibility, low usage of organic solvents, low cost, and short extraction time are some of the considerable features of SPE, which make this technique superior to other conventional methods. Furthermore, adsorbents can be regenerated by desorption processes and reused [13].

It should be noticed that the success of SPE relies on the choice of an appropriate adsorbent. In this respect, MNPs have been engaged for supporting functionalities with coordination ability to toxic metal ions [14]. During the last decades, magnetite nanoparticles (MNPs) have attracted much attention in the catalysis area owing to their stability, low toxicity and cost, high dispersibility, good biocompatibility, and high surface-to-volume ratio [15-19].

Among the wide range of chemical procedures that deal with the extraction of metal ions from aqueous media, surface-functionalized MNPs with metal coordinating ligands have attracted increasing interest. For example, Lin et al. [8] prepared magnetic polymer beads containing amino groups on their surfaces in order to enable them to capture Cu(II), Ni(II), and Co(II) cations from aqueous solutions. They observed the highest adsorption capacities over the pH range of 3 to 5, with slight temperature dependence. The clearance and regeneration efficiencies of their magnetic adsorbent were reported to be higher than 98%. Separation of rare-earth ions by surface-treated MNPs, SiO_2, and TiO_2 NPs with N-[(3-trimethoxysilyl)propyl]ethylenediamine triacetic acid (TMS-EDTA) has been reported by Dupont et al. [20]. Enhanced metal uptake capacities (100 to 400 mg g^{-1}) of the investigated NPs are attributed to the small diameter and high surface area. They claimed that silica and titania NPs could be loaded by higher amounts of TMS-EDTA and, therefore, larger quantities of rare-earth ions can be adsorbed, but their removal from solutions is very tedious. Jainae et al. [21] prepared thiol-functionalized polystyrene-coated magnetic $CoFe_2O_4$ NPs for selective adsorption of Hg(II) cations. By employing a concentrated Hg(II) solution (100 ppm), to ensure full coverage of Hg(II) ions, they reported the metal uptake capacity of 89.6 mg g^{-1} and ten cycles of usage. Qiu et al. [22] reported simultaneous detection and removal of low Cu(II) concentrations by a magnetic nanocomposite modified by a selective chelating group with the removal efficiency of 80% and 27.5 mg g^{-1} adsorption capacity. Recently, Chen et al. reported removal of Co(II) and Ni(II) aqueous solution using reductive self-assembly of three-dimensional magnetic fungal hyphal/graphene oxide nanofibers [23]. A continuous-flow recycle reactor was also proposed for emergency aqueous solution treatment. Wang et al. used carboxymethylcellulose-chitosan film modified magnetic alkaline Ca-bentonite for the efficient removal of Pb(II) and Cd(II) from aqueous solution. The sorbent could be efficiently recycled with less decrease in adsorption capacity [24].

In this study, a birhodanine containing silane compound, i.e. [(E)-5-(3-(3-(trimethoxysilyl)propyl)-4-oxo-2-thioxothiazolidin-5-ylidene)-3-phenethyl-2-thioxothiazolidin-4-one] (TMOS-BIRD), is studied to modify the adsorbent's surface. Diverse biological activities through inhibition of numerous targets, e.g., HIV-1, Alzheimer's disease, HCV NS3 protease, b-lactamase, PMT1 mannosyl transferase, PRL-3, and JSP-1 phosphatases are reported for rhodanine-based molecules [25, 26]. Rhodanine heterocycle can also coordinate with metal ions due to the presence of thioamide and keto groups. In a study, Song et al. [27] grafted polyrhodanine onto the inner surface of an anodic alumina membrane to remve mercury, lead, and silver ions. They attributed the maximum removal capacity (7.01 mmol/g polymer) to Ag(I) cations. Lee et al. [28] prepared rhodanine-loaded poly(methylmethacrylate) electrospun nanofibrous membranes to remove heavy metal ions. Their experimental results suggested that their prepared membranes exhibit good ion uptake capabilities for Ag(I) and Pb(II) cations. Amiri et al. [29] proposed chitosan/polyrhodanine nanocomposite particles to eliminate Ni(II) ions from aqueous solutions. Their observed adsorption trend followed pseudo-second-order kinetics and gave the maximum equilibrium uptakes of 61.43 and 67.70 mg g^{-1}, obtained from the Langmuir and Sips isotherms, respectively. Chen et al. [30] used self-assembly of rhodanine/gold NPs to construct a colorimetric sensing device for Hg(II) detection in aqueous media. The aggregation of NPs is induced by Hg(II) ions, and a color change from wine red to blue is observed. Based on the experimental results, particle aggregation is due to the formation of the $[Hg(rhodanine)_2]^{2+}$ adduct.

We reported the preparation of a rhodanine-based monomer. The monomer was polymerized on MNPs via the SI-ATRP approach [31]. The polymer grafted NPs were used to quickly eliminate Co(II) ions, and 86.0% of Co(II) ions were removed in only 7 min.

Birhodanine compounds with the exact IUPAC name of 2,2'-dithioxo-[5,5']bithiazolidinylidene-4,4'-dione) are an interesting group of rhodanine-based derivatives and can be synthesized through various routes [32-34]. The use of these organic heterocycles has been extended to numerous applications, such as dyes [35], transistors [36], catalysts [37], polymers, and nanocomposites [38]. In this work, we wish to report the design and synthesis of a new birhodanine compound for surface silylation. The prepared compound has two structural rhodanine heterocycles. It can merge enhanced coordinating activity with easy surface anchoring procedure on metal oxides to produce novel heterogeneous adsorbents for removal of metal ions. It must be noted, ease of hydrolytic cleavage of rhodanine nucleus in alkaline media limits the incorporation of the supported catalyst to neural and weak acidic solutions [38]. This can be considered as the main disadvantage of the supported adsorbent. To the best of our knowledge, the present study is the first report on the immobilization of rhodanine moiety via silylation.

Following our approach reported for one-pot synthesis of birhodanine compounds under solvent-free condition [39, 40], and considering the rhodanine ring's ability towards coordinating to metal ions, we thought that anchoring this structure on the surface of MNPs might be invaluable for the removal of metal ions. Therefore, in this work, we report the preparation and characterization of a new birhodanine containing silylating compound (TMOS-BIRD; Fig. 1) that can be incorporate for surface silylation of metal oxides such as MNPs.

The adsorption performance of the prepared MNPs was assessed via removing Co(II) cations from aqueous solutions. Also, the kinetics and thermodynamics of adsorption are investigated under optimal conditions. Furthermore, the Langmuir and Freundlich isotherms are employed to fit the experimental adsorption data.

MATERIALS AND METHODS

Synthesis of the silylating birhodanine compound (TMOS-BIRD)

A mixture of APTMS (0.358 g, 1 mmol), carbon disulfide (0.304 g, 4 mmol), compound VI (0.616 g, 2 mmol) and a catalytic amount of tetrabutylammonium bromide (TBAB) (0.128 g, 0.4 mmol) was stirred for 1 h at room temperature, under solvent-free condition. Then, water (8 ml) and dichloromethane (32 ml) were added. The organic layer was evaporated after drying over anhydrous calcium chloride, and the crude product was recrystallized from EtOH to afford 0.316 g golden crystals (Yield: 30%) [40]. m.p. 205-207°C. FTIR (KBr, cm^{-1}): 2927 (m), 1695 (s), 1428 (m), 1349 (s), 1176 (s), 1086 (s), 870 (m), 743 (m),

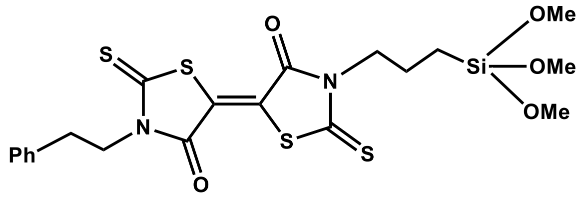

Fig. 1. Chemical structure of TMOS-BIRD.

699 (m). ^{1}H-NMR (250 MHz, $CDCl_3$) δ: 7.26-7.31 (m, J =5 Hz, 5H), 4.33 (t, J =7.5 Hz, 2H), 4.11 (t, J =7.5 Hz, 2H), 3.56 (s, 9H), 2.99 (t, J =7.8 Hz, 2H), 1.70-2.00 (m, 2H), 0.67 (t, J =7.5 Hz, 2H) ppm. ^{13}C NMR (62.5 MHz, $CDCl_3$) δ: 194.2, 166.6, 136.8, 128.7, 127.0, 124.9, 124.3, 50.6, 46.7, 45.6, 33.0, 20.5, 13.7, 6.5 ppm.

Silylation of magnetite and synthesis of MNP@ BIRD NPs

TMOS-BIRD (0.700 g, 1.3 mmol) was added to a dispersion of MNPs (0.600 g in 30 ml) in 6.0 ml of 2M triethylamine solution in toluene and stirred for 24 h under argon at room temperature. The silylated MNPs were decanted magnetically and washed thoroughly with MeOH. Removal of any un-reacted TMOS-BIRD was ensured by repeating the washing procedure three times, and finally, the silylated NPs were dried in a vacuum [41, 42].

Adsorption study

Adsorption investigations were accomplished by the batch technique in the dispersion of MNP@ BIRD NPs in aqueous solutions of Co(II) ions. NaOH and HCl (0.1 M) were used to adjust the pH of aqueous solutions. The details of adsorption study, kinetic study, equilibrium isotherms, thermodynamic assessment, and desorption experiments were explained in the supporting information file.

RESULTS AND DISCUSSION

Synthesis and characterization of MNP@BIRD NPs

The silylating birhodanine compound, i.e., TMOS-BIRD or compound (VI), was prepared according to Fig. 2, and it was used for the silylation of MNPs. Methyl 2-(4-oxo-3-phenethyl-2-thioxothiazolidin-5-ylidene)acetate (IV) was easily obtained (55 % yield) through the one-pot three-component reaction of 4-phenethylamine (II), carbon disulfide (I), and DMAD (III) in water at room temperature [43]. Compound IV was further reacted with carbon disulfide (I) and APTMS (V) in the presence of TBAB at room temperature under solvent-free conditions to give TMOS-BIRD (VI).

The ^{1}H NMR and ^{13}C NMR spectra of TMOS-BIRD are exhibited in Figs. 3a and 3b, respectively. The aromatic ring protons of TMOS-BIRD appeared at 7.20 to 7.40 ppm, and the protons related to the methylene groups are distinguished with the expected multiplicities, Fig. 3a. In Fig. 3b, 16 signals are observed that are consistent with the structure of TMOS-BIRD. In the mass spectrum (Fig. 4), molecular ion peak is appeared at m/e = 528.2 (4%).

As aforementioned above, MNP@BIRD NPs were obtained through silylation of MNPs by TMOS-BIRD. The FTIR spectra of MNPs, MNP@ BIRD NPs, and TMOS-BIRD are shown in Figs. 5a to 5c, respectively. In the FTIR spectrum of MNP@ BIRD NPs (Fig. 6b), the appearance of the 3030

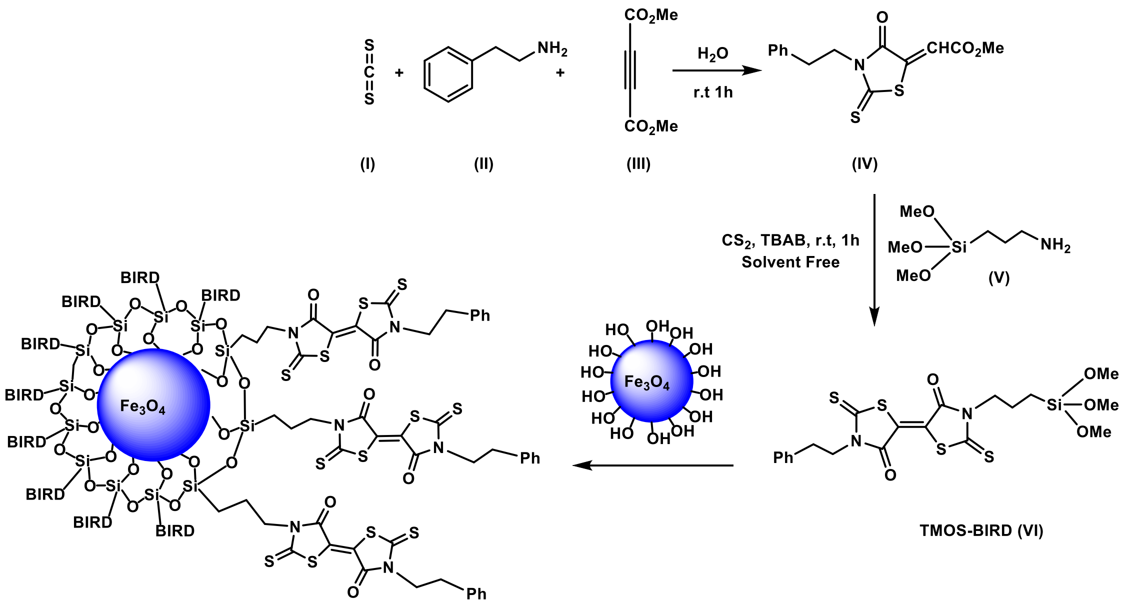

Fig. 2. Synthesis of MNP@BIRD NPs.

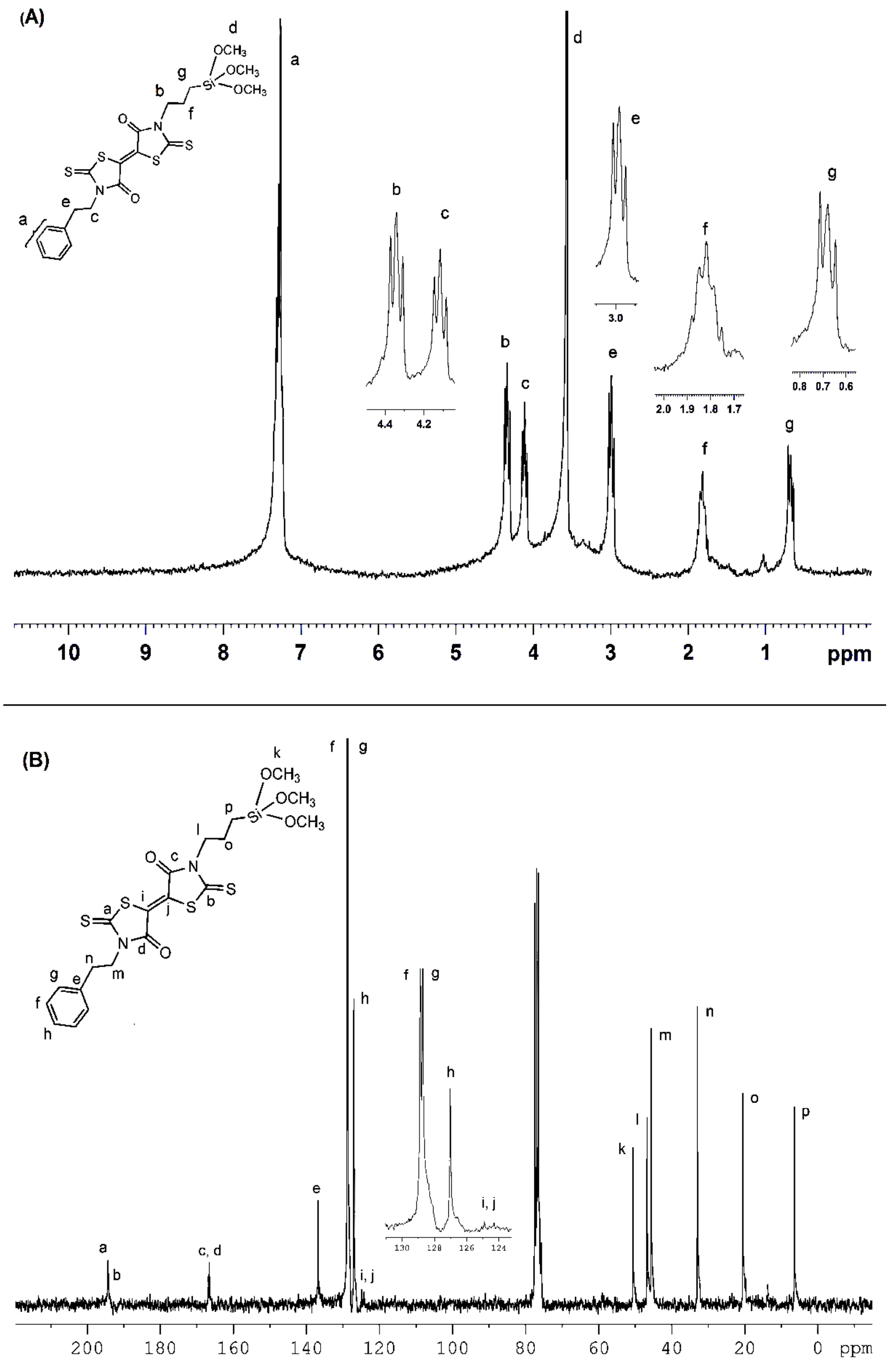

Fig. 3. A) [1]H NMR (250 MHz, $CDCl_3$); and B) [13]C NMR (62.5 MHz, $CDCl_3$) of TMOS-BIRD.

cm^{-1} (ν_s arom. C-H), 2928 cm^{-1} (ν_s CH_2), 1696 cm^{-1} (C=O stretching), and 1428 cm^{-1} (CH_2 bending) transmittance bands, along with the rhodanine ring related vibrations at 1350, 1262 and 1176 cm^{-1}, clearly confirms silylation of MNPs by TMOS-BIRD. The presence of the siloxane vibrational mode (ν_{as}

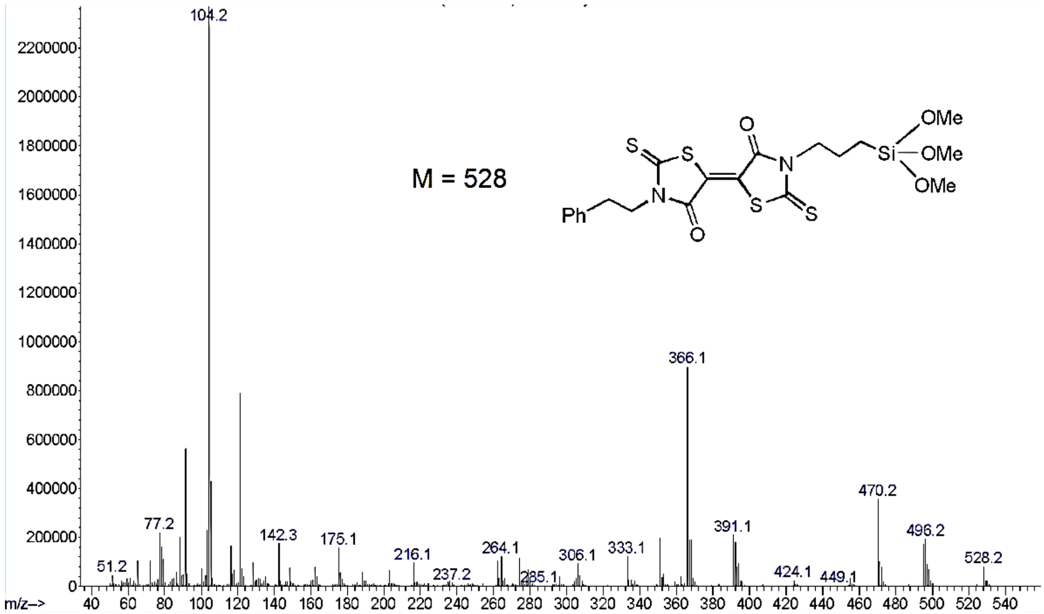

Fig. 4. Mass spectrum of TMOS-BIRD.

Si-O-Si) at 1112 cm^{-1} beside the characteristic peak of magnetite at 588 cm^{-1} (44) confirms the success of the silylation reaction and formation of MNP@BIRD core-shell.

In the SEM image of MNP@BIRD NPs, the spherical morphology of 20-30 nm diameter can be distinguished, Fig. 6. The TEM image of MNP@BIRD reveals spherical or ellipsoidal-

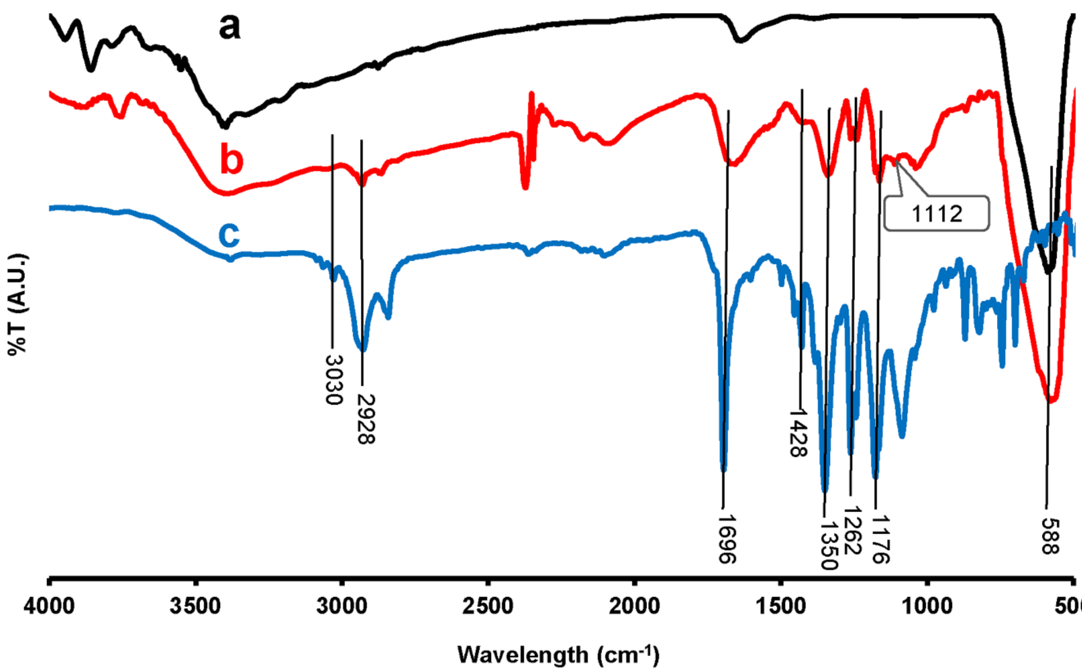

Fig. 5. The comparative FTIR spectra of: (a) MNPs; (b) MNP@BIRD NPs; and (c) BIRD.

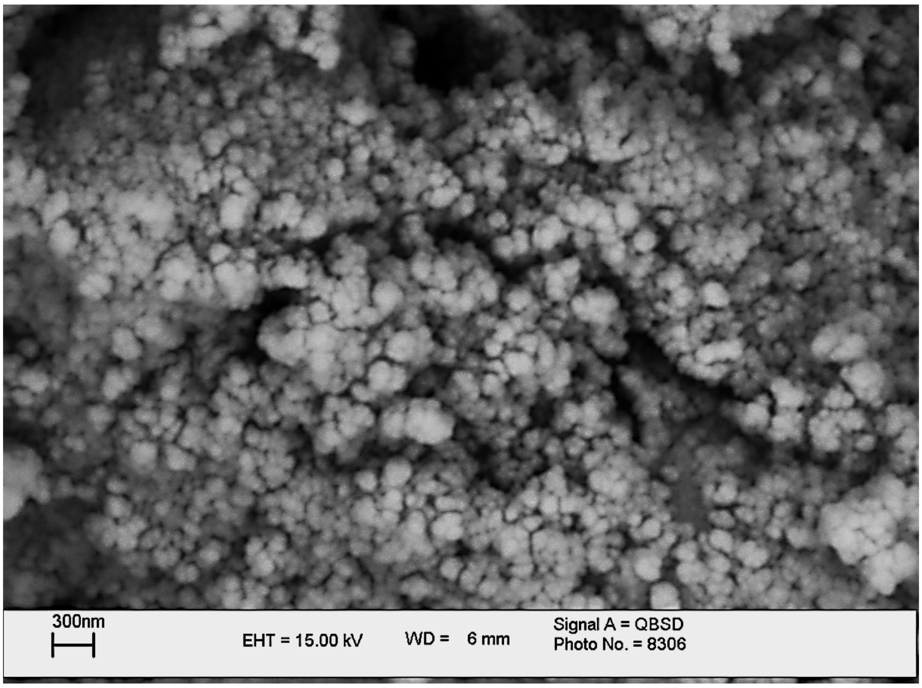

Fig. 6. The SEM image of MNP@BIRD NPs.

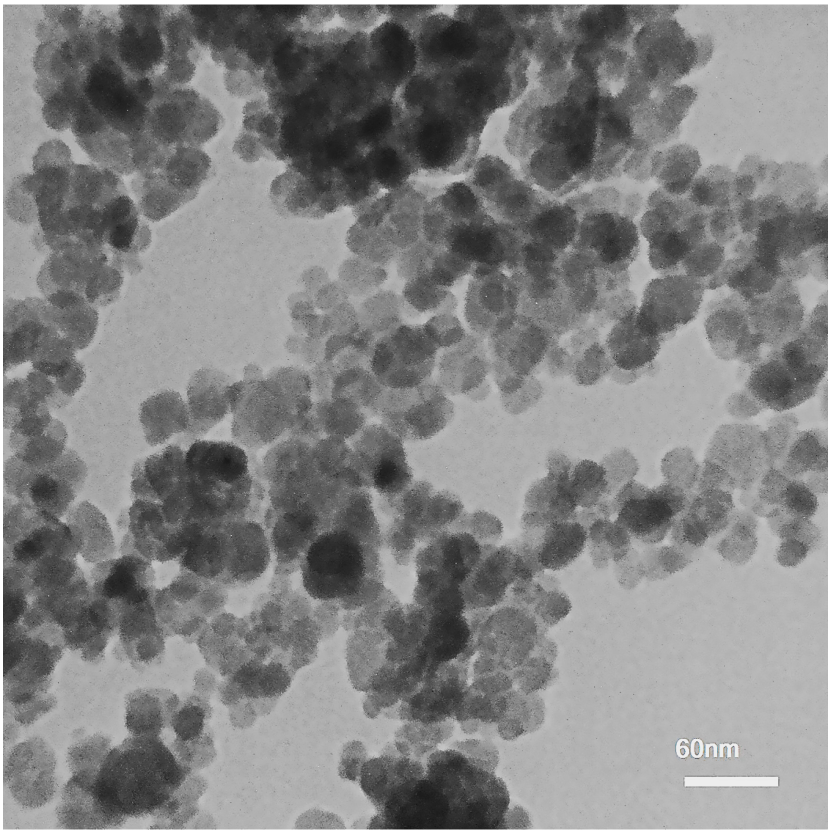

Fig. 7. The TEM image of MNP@BIRD NPs.

BIRD NPs were depicted in Fig. 10. The saturation magnetization (M_s) of MNPs and MNP@BIRD NPs are 69.5 and 78.1 emu/g, respectively. The obtained values are less than the value reported for bulk Fe_3O_4 particles [47]. Therefore, the prepared MNPs are superparamagnetic, and covering MNPs by a non-magnetic silica layer is responsible for decreasing of M_s value for MNP@BIRD NPs. Moreover, the small field coercivity of MNP@BIRD NPs (H_c = 36.5 Oe) shows that the prepared NPs are superparamagnetic [48]. Therefore, the magnetization of MNPs did not affect significantly by the silylation reaction. The results for magnetization measurements are

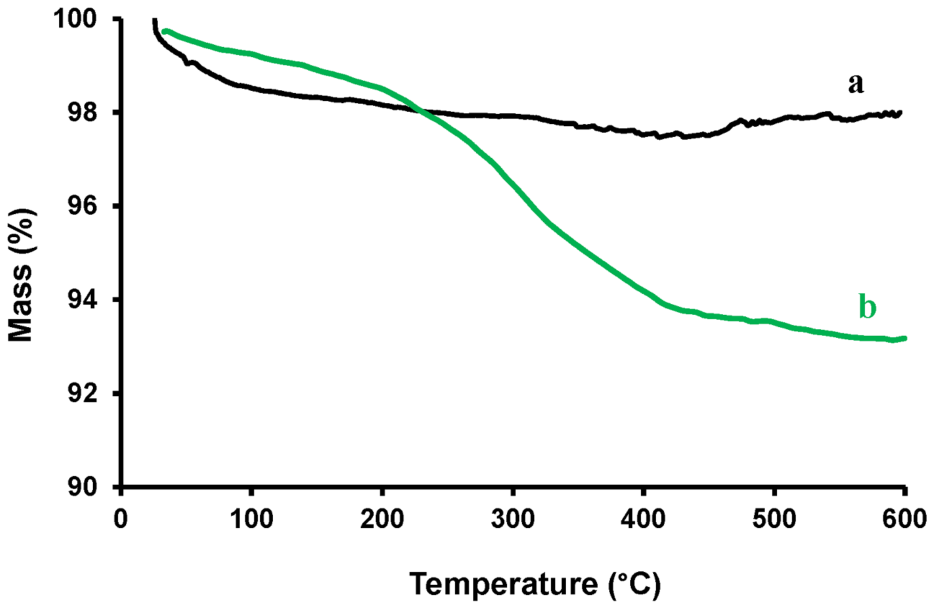

Fig. 8. TGA thermograms (N_2 atmosphere, scan rate of 10ºC/min) of: a) MNP@BIRD NPs; (b) and MNPs.

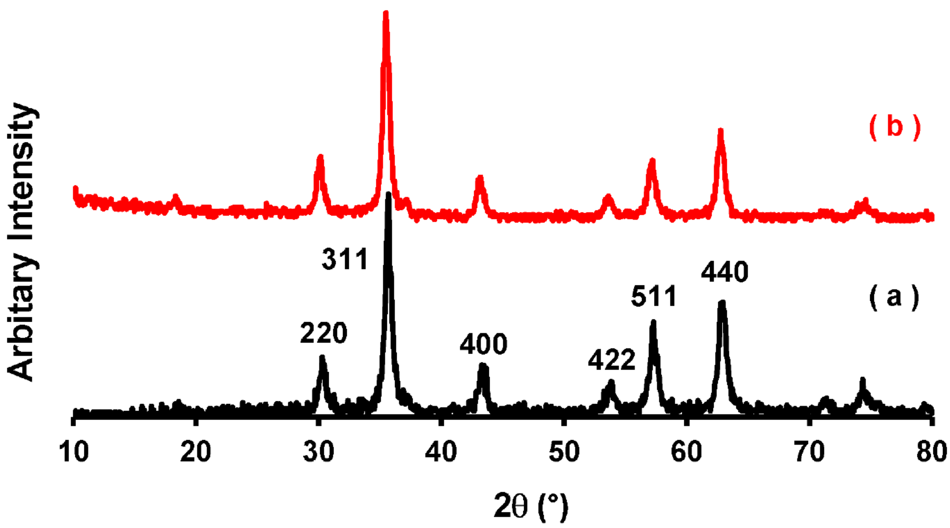

Fig. 9. WXRD patterns of: (a) MNPs and; (b) MNP@BIRD NPs.

summarized in Table 1.

Adsorption Study

Rhodanine compounds contain several potential coordinating sites to attach to different metallic ions [49, 50]. Therefore, immobilization of rhodanine derivatives onto magnetic substrates for removing toxic heavy metal ions from water or wastewater is worthful. To demonstrate the efficiency of the prepared adsorbent for Co(II) removal, MNP@BIRD NPs were added to the solution of Co(II) ions at room temperature and then collected by an external magnet. Figs. 11a and 11b show the FTIR spectra of MNP@BIRD NPs and the Co(II) complexed adsorbent, respectively. The frequency related to C=O stretching in the Co(II) complexed adsorbent shows a very distinct shift (by 30 cm^{-1}) and appeared at 1638 cm^{-1}. The observed red shift is due to the weakening of the C=O bond upon coordination, which lowers the stretching frequency. The possible coordination of Co(II) ions to the supported birhodanine moieties is demonstrated in Fig. 12.

Metal removal can also be observed visually by receding the purple colour of the solution after magnetic decantation, Figs. 13a-c. The optimal adsorption conditions were determined in order to investigate the corresponding adsorption kinetics and thermodynamics. Contact time of 30 min, pH 8, initial metal ion concentration of 3.0 ppm, and 10 mg of the adsorbent were chosen as the best conditions for Co(II) removal from a 25 ml aqueous

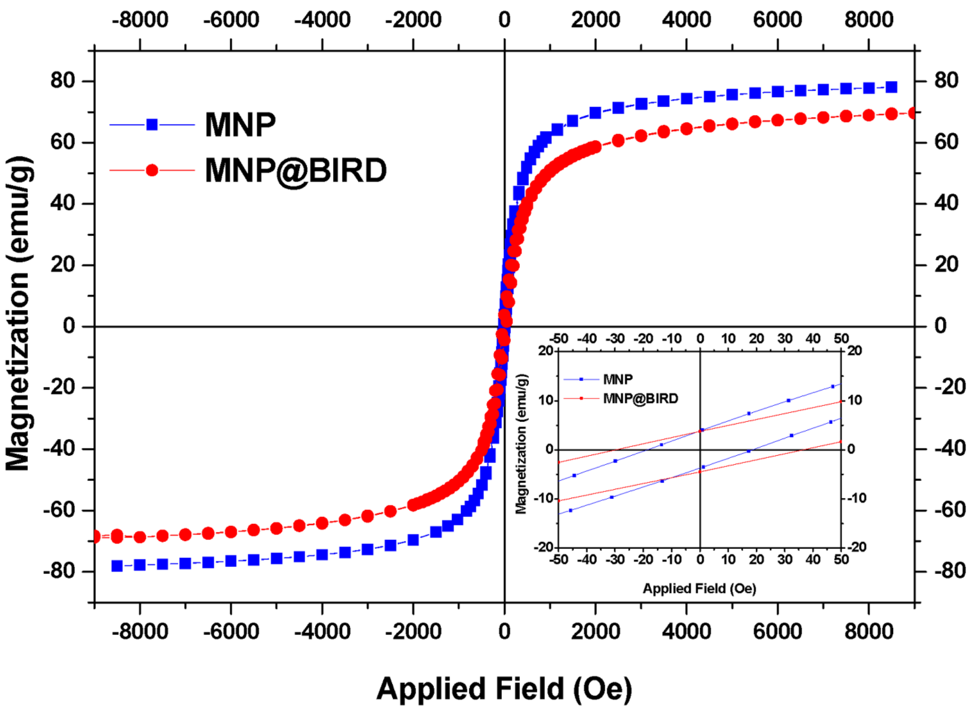

Fig. 10. Magnetization curves for MNPs and MNP@BIRD NPs at room temperature.

Table 1. Magnetic properties of MNPs and MNP@BIRD NPs.

Sample	[a] M_s (emu g^{-1})	[b] M_r (emu g^{-1})	[c] H_c (Oe)	[d] M_r/M_s
MNP	78.1	3.8	18.6	0.05
MNP@BIRD	69.5	3.8	36.5	0.05

[a] Saturation magnetization. [b] Remanent magnetization. [c] Coercive force. [d] Remanence ratio.

shaped NPs of uniform size distribution, Fig. 7. Therefore, the prepared MNP@BIRD NPs are superparamagnetic, and their size distribution is equal to the recommended critical value (25 nm) for biomedical applications [44, 45]. As seen in Fig. 7, MNPs are covered by a silica layer of about 10.1 nm diameter. Twenty selected random particles in a TEM Image were used to determine the silica layer thickness by ImageJ software.

TGA was used to estimation of the loaded amount of the sorbent. Water removal is shown by a mass loss of about 2.0% for the bare MNPs from ambient temperature to 600ºC, Fig. 8a. TGA curve of MNP@BIRD exhibits a mass loss of about 6.8% under a similar condition due to thermolysis of the birhodanine moiety, Fig. 8b. The difference between these two values (Δm = 4.8%) can be attributed to the amount of grafted birhodanine molecules onto MNPs (4.8% or 48 mg g^{-1} of MNPs).

The XRD patterns of the bare MNPs and core-shell of MNP@BIRD are presented in Figs. 9a and 10b. Both samples exhibit the characteristic peaks of cubic Fe_3O_4 with the Fd-3m space group [46]. Therefore, the spinel lattice structure of magnetite is retained. The reduction of peak intensities can be attributed to the coating of MNPs by an amorphous silica layer, Fig. 9b.

The hysteresis curves of MNPs and MNP@

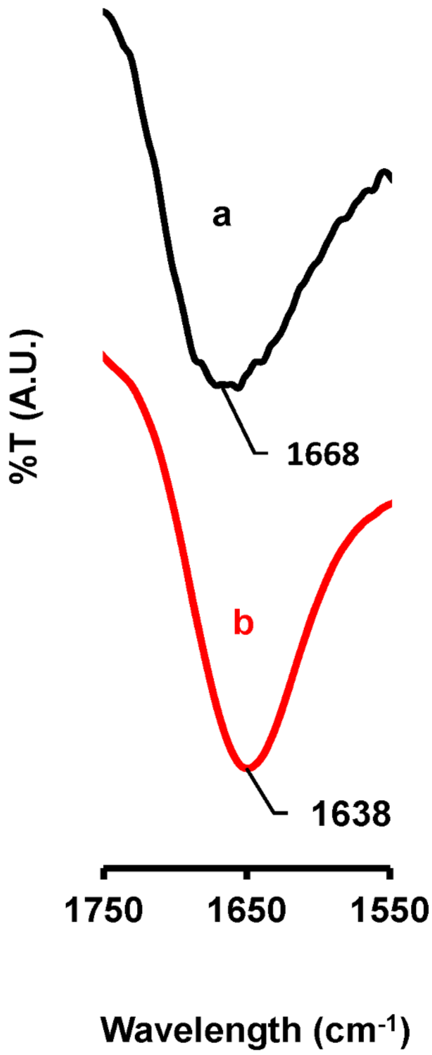

Fig. 11. Portion FTIR spectra of: a) MNP@BIRD NPs and; (b) MNP@BIRD-Co(II) complexed NPs.

solution. The details of the optimization trials were described in the Supporting Information file.

The Study of Adsorption Kinetics

Figs. 14a and 14b show the experimental results of the kinetic investigation. Lagergren's pseudo-first-order (Eq. 1) and Ho's pseudo-second-order (Eq. 2) models were applied to fit the adsorption kinetic data [41].

$$\ln(Q_e - Q_t) = lnQ_e - k_f t \quad (1)$$

$$\frac{t}{Q_t} = \frac{1}{k_s Q_e^2} + \frac{1}{Q_e} t \quad (2)$$

where k_f (1/min) and k_s (g/(mg. min)) are the pseudo-first-order and pseudo-second-order equilibrium rate constants, respectively. Q_e and Q_t are adsorbed metal ions (mg g^{-1}) at equilibrium and time t, respectively. For the pseudo-first-order model, Q_e, k_f, and correlation coefficient obtain from the linear plot of ln (Q_e - Q_t) against t, Fig. 14a. The correspondent values for pseudo-second-order equilibrium (Q_e, k_s, and R^2) obtain from the plot of t/Q_t versus t, Fig. 14b. The results are summarized in Table 2. As can be seen, the pseudo-first-order model is better fitted with the experimental data than that of the pseudo-second-order model. Furthermore, the calculated and experimental values of adsorption capacity ($Q_{e,cal}$ and $Q_{e,exp}$) are more consistent in the case of

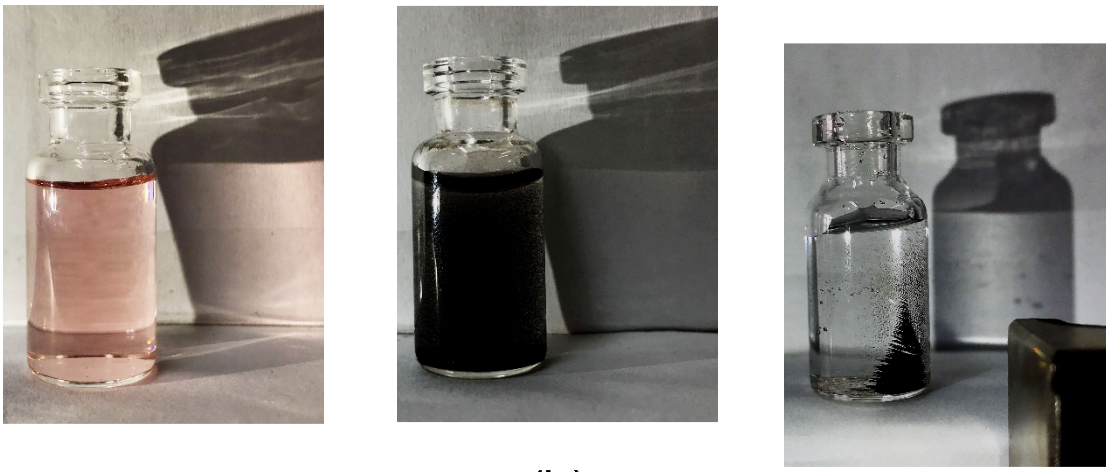

(a) (b) (c)

Fig. 13. Photographs of Co(II) removal by MNP@BIRD NPs: (a) aqueous Co(II) solution (b) aqueous Co(II) solution treated by MNP@ BIRD NPs, (c) after 30 min of adsorption and magnetic separation of the adsorbent.

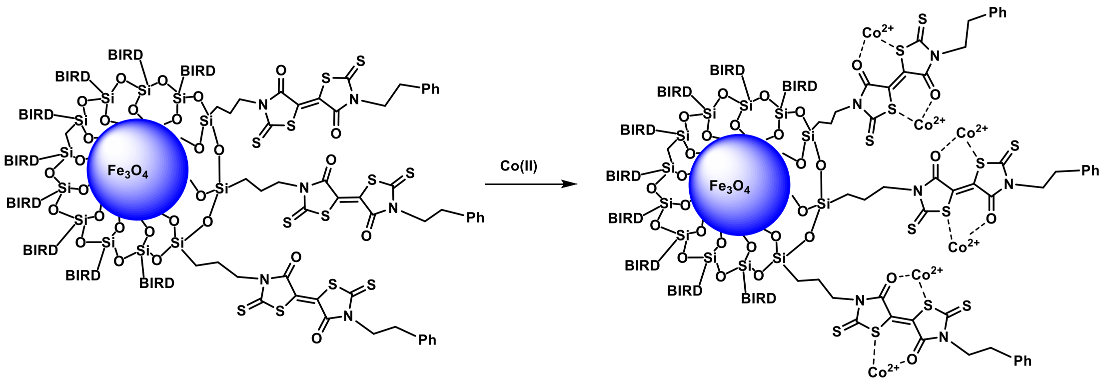

Fig. 12. Coordination of Co(II) ions to MNP@BIRD NPs.

the pseudo-first-order model ($Q_{e,exp}$ = 5.36 mg g^{-1}, $Q_{e,cal}$ = 6.71 mg g^{-1}).

Adsorption isotherm studies

The adsorption parameters were found by fitting the experimental results with the Langmuir and Freundlich isotherm models. The isotherm model that best fitted the experimental data was then used to calculate the adsorption parameters. According to the Langmuir model, the binding

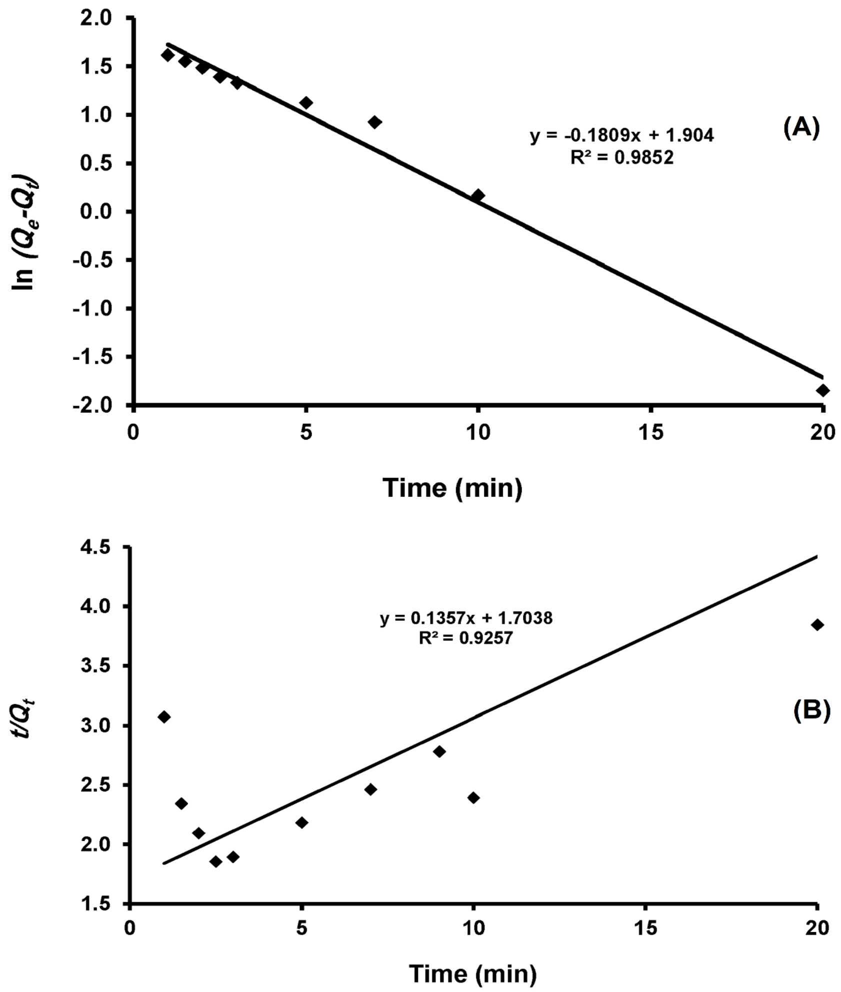

Fig. 14. Pseudo-first-order kinetics (A) and pseudo-second-order kinetics (B) of Co(II) adsorption on MNP@BIRD NPs; initial Co(II) concentration 3.0 ppm, pH = 8.0, Sorbent mass 10 mg, Solution volume 25 ml.

Table 2. Adsorption kinetics parameters of MNP@BIRD NPs.

	Kinetic Model					
	Pseudo 1st order			Pseudo 2Nd order		
$Q_{e,exp}$ (mg g^{-1})	$Q_{e,cal}$ (mg g^{-1})	k_f (min^{-1})	[a] R^2	$Q_{e,cal}$ (mg g^{-1})	k_s (g/(mg. min))	[a] R^2
5.36	6.71	0.18	0.9852	7.37	0.01	0.9257

[a] Correlation coefficient

sites of the adsorbent are identical. The adsorbed molecules are single-site located, and they have not any interaction with other molecules. Therefore, adsorbate species form a monolayer on the surface. The linear form of Langmuir isotherm can be written as Eq. 3:

$$\frac{C_e}{Q_e} = \frac{1}{Q_m K_L} + \frac{C_e}{Q_m} \quad (3)$$

where C_e, Q_e, Q_m, and K_L are Co(II) equilibrium

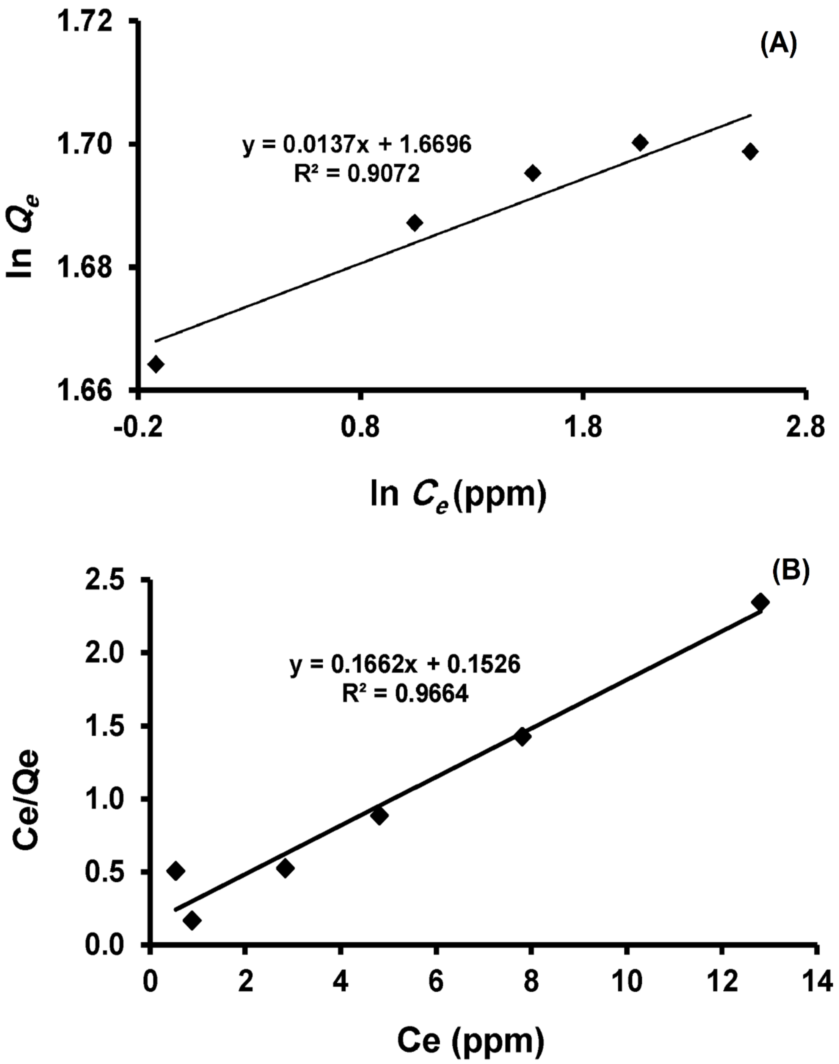

Fig. 15. Langmuir isotherm (A) and Freundlich isotherm (B) plots to remove Co(II) cations by MNP@ BIRD NPs; pH = 8, Sorbent mass 10 mg, Solution volume 25 ml.

Table 3. Langmuir and Freundlich adsorption isotherm parameters to remove Co(II) cations.

Langmuir isotherm constants				Freundlich isotherm constants			
$Q_{e.exp}$ (mg g^{-1})	Q_m (mg g^{-1})	$^aR^2$	R_L	K_L (L/mg)	$^aR^2$	$1/n$	K_F ((mg g^{-1})(L/mg)$^{1/n}$)
5.36	6.02	0.9964	0.06-0.66	1.09	0.9072	0.01	5.31

[a] Correlation coefficient

concentration (mg/L), adsorbed metal ion at equilibrium (mg g^{-1}), the maximum capacity for Co(II) uptake (mg g^{-1}), and the Langmuir adsorption constant (L/mg), respectively. Q_m and K_L are the Langmuir model parameters and obtain from the linear plot of C_e/Q_e against C_e.

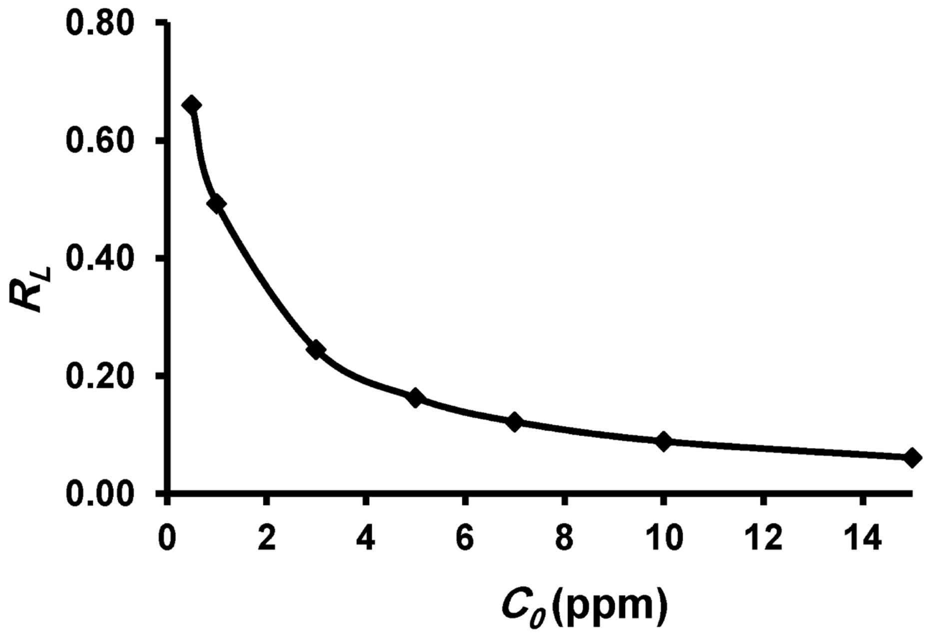

Fig. 16. Separation factor to remove Co(II) cations by MNP@BIRD NPs. Sorbent mass 10 mg, pH = 8.0, Solution volume 25 ml, t = 30 min, C_0 = 0.5-15.0 ppm.

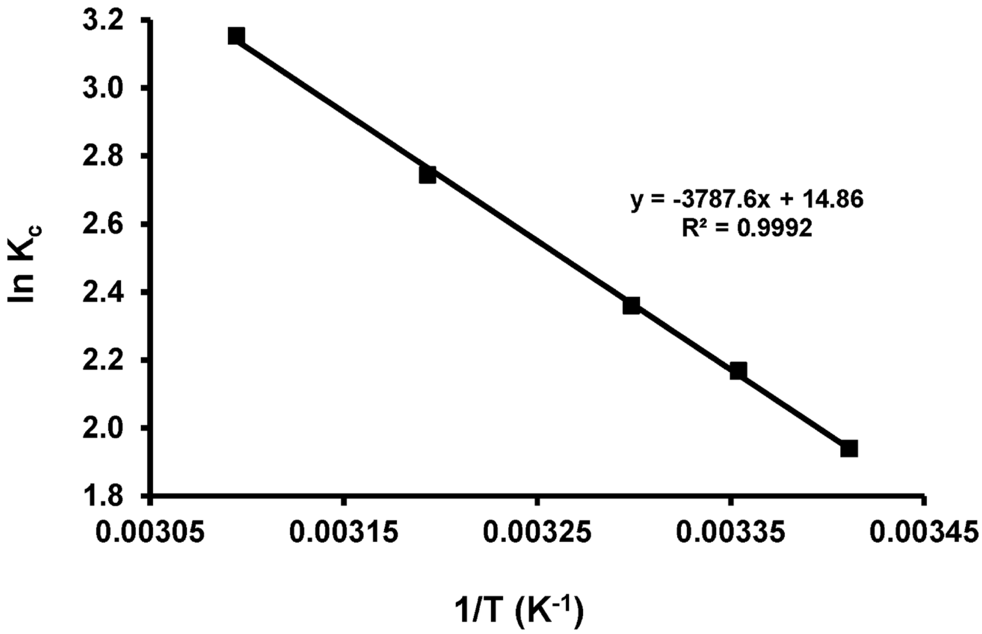

Fig. 17. Estimation of thermodynamic parameter for Co(II) removal by MNP@BIRD NPs. Initial Co(II) concentration 3.0 ppm, pH = 8.0, t = 30 min, Sorbent mass 10 mg, Solution volume 25 ml.

The linear form of Freundlich isotherm is written as Eq. 4:

$$\ln Q_e = lnK_F + \frac{1}{n} lnC_e \quad (4)$$

where Q_e is the adsorbed Co(II) ions onto the sorbent at equilibrium (mg g^{-1}), C_e is the Co(II) concentration at equilibrium (mg/L), and K_F is the Freundlich isotherm constant ((mg g^{-1})(L/mg)$^{1/n}$). The values of K_F and 1/n (sorption intensity) obtain from the linear plot of ln Q_e vs. ln C_e [51].

The plots for Langmuir and Freundlich isotherms are shown in Figs. 15a and 15b, respectively. The related parameters are also listed in Table 3. As can be seen, Langmuir isotherm shows better compatibility with the experimental data (R^2 = 0.9964) than the Freundlich isotherm (R^2 = 0.9072). This implies that a layer of the metal ions covers the MNP@BIRD surface. The maximum adsorption capacities, obtained from the Langmuir (Q_m = 6.02 mg g^{-1}) and Freundlich (K_F = 5.31 mg g^{-1}) models, are both following the experimental value ($Q_{e.exp}$ = 5.36 mg g^{-1}). Fig. 16 presents the calculated R_L values at different initial Co(II) concentrations, and the results are summarized in Table 3. As seen, the R_L values are in the range of 0 and 1. This means that the adsorption Co(II) ions on MNP@BIRD NPs is a favorable process [52].

Adsorption thermodynamics

Thermodynamic parameters are essential for a practical application because they provide

Table 4. Thermodynamic parameters for adsorption Co(II) ions on MNPs@BIRD NPs.

ΔH (Kj mol^{-1})	ΔS (J mol^{-1}.K^{-1})	ΔG (Kj mol^{-1})				
		20°C	25°C	30°C	40°C	50°C
30.81	123.55	-4.73	-5.37	-5.95	-7.15	-8.47

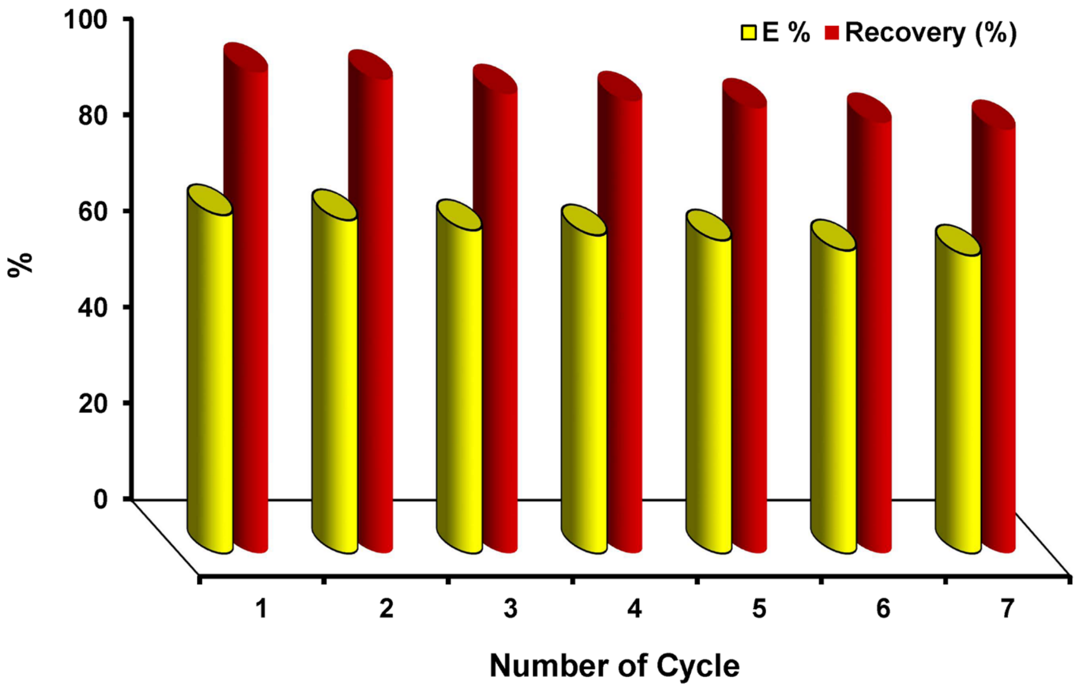

Fig. 18. Recyclability of MNP@BIRD NPs; initial Co(II) concentration 3.0 ppm, pH = 8.0, t = 30 min, Sorbent mass 10 mg, Solution volume 25 ml.

Table 5. Adsorption capacity of MNP@BIRD for Co(II) adsorption.

Adsorbents	Adsorption Capacity Q_m (mg g^{-1})	Reference
ACRH	0.02	(53)
Magnetite	0.11	(54)
Kaolinite	0.92	(55)
Granular activated carbon	1.19	(56)
Palygorskite	8.88	(57)
MWCNT/IO	8.85	(58)
Chitosan	0.48	(59)
Attapulgite	2.50	(57)
Magnetic chitosan (MCS)	2.98	(60)
$SiO_2/Nb_2O_5/ZnO$	0.52	(61)
SDMA	9.90	(22)
Chitosan/Vanillin	5.90	(62)
Chitosan/*o*-Vanillin	7.65	(62)
MNP@BIRD	6.71	This work

useful information about the nature of surfaces and adsorbed phases. In general, ΔH and ΔS values can be calculated from Eqs. 5 and 6:

$$\ln K_C = -\frac{\Delta G}{RT} \quad (5)$$

$$\ln K_C = \frac{\Delta S}{R} - \frac{\Delta H}{RT} \quad (6)$$

where K_C, R, and T are the equilibrium constant, the gas constant (8.314 J/(mol.K)), and absolute temperature (K), respectively. The values of ΔH and ΔS were derived from the linear plot of ln K_C against 1/T, which is presented in Fig. 17.

ΔG can be obtained from Eq. 7.

$$\Delta G = -RT\ln K_C \quad (7)$$

The results of the thermodynamic investigation are summarized in Table 4. Positivity of the ΔH value indicates the endothermic nature of Co(II) adsorption onto MNP@BIRD NPs, whereas the positive ΔS value declares the increase of randomness at the solid/liquid interface during SPE of Co(II) ions. Releasing of water molecules around the hydration sphere of Co(II) ions upon adsorption of the solvated metal ions is responsible for the positive ΔS value. Meantime, the negative ΔG values reveal that the adsorption process is spontaneous. Therefore, ΔG is mainly influenced by TΔS, and increasing entropy favors the adsorbent interaction with the metal ions [10].

Recyclability of the sorbent

Preparing a synthetic adsorbent is usually done via a complicated process. Therefore, sufficient attention to the recycling of a used sorbent is necessary. In the present study, regeneration of the used MNP@BIRD NPs was done by treating the used adsorbent with the diluted aqueous HCl solution followed by neutralization and washing steps. As shown in Fig. 18, the values of extraction efficiency (E %) and recovery % were not changed significantly after seven consecutive runs. The average extraction efficiency (E %) reached to 62.0% (89.1 % recovery) after seven cycles.

The adsorption capacity of MNP@BIRD NPs is compared with a few literature-reported adsorbents in Table 5. Comparison of the outlined adsorption capacities demonstrates that in the most cases, the prepared NPs are more effective than the reported adsorbent (Q_m = 6.02 mg g^{-1}). The obtained NPs also enjoy magnetic decantation as the main advantage.

CONCLUSION

The synthesis and characterization TMOS-BIRD as a new silylating agent for the silylation of MNPs have been reported. TGA experiments reveal that the birhodanine content of the prepared NPs was 48 mg g^{-1}. The prepared MNP@BIRD NPs were used for magnetic deionization of the aqueous solutions from Co(II) ions. The calculated metal adsorption capacity was 6.02 mg g^{-1}, and the experimental data obeys the pseudo-first-order kinetics and Langmuir isotherm model. Thermodynamic investigation revealed the endothermic and spontaneous nature of the adsorption process. The recyclability of the prepared sorbent was shown at least seven times. Based on the obtained results, it can be suggested that MNP@BIRD NPs are stable, reusable, and can be efficiently used in water and wastewater treatment processes.

ACKNOWLEDGEMENT

The Graduate Council of the University of Mohaghegh Ardabili is gratefully acknowledged for providing the financial support. This work was supported by University of Mohaghegh Ardabili (Grant number 222/13D/94).

CONFLICT OF INTEREST

The authors declare that there is no conflict of interests regarding the publication of this manuscript.

REFERENCES

1. Azizi P, Golshekan M, Shariati S, Rahchamani J. Solid phase extraction of Cu^{2+}, Ni^{2+}, and Co^{2+} ions by a new magnetic nano-composite: excellent reactivity combined with facile extraction and determination. Environmental Monitoring and Assessment. 2015;187(4).
2. Kurniawan TA, Chan GYS, Lo W-h, Babel S. Comparisons of low-cost adsorbents for treating wastewaters laden with heavy metals. Sci Total Environ. 2006;366(2-3):409-426.
3. Strachan S. Trace elements. Current Anaesthesia & Critical Care. 2010;21(1):44-48.
4. Xing M, Wang J. Nanoscaled zero valent iron/graphene composite as an efficient adsorbent for Co(II) removal from aqueous solution. Journal of Colloid and Interface Science. 2016;474:119-128.
5. Simonsen LO, Harbak H, Bennekou P. Cobalt metabolism and toxicology—A brief update. Sci Total Environ. 2012;432:210-215.
6. Behl M, Stout MD, Herbert RA, Dill JA, Baker GL, Hayden BK, et al. Comparative toxicity and carcinogenicity of soluble and insoluble cobalt compounds. Toxicology. 2015;333:195-205.
7. SenthilKumar P, Ramalingam S, Abhinaya RV, Kirupha SD, Vidhyadevi T, Sivanesan S. Adsorption equilibrium, thermodynamics, kinetics, mechanism and process design of zinc(II) ions onto cashew nut shell. The Canadian Journal of Chemical Engineering. 2011;90(4):973-982.
8. Lin Z, Zhang Y, Chen Y, Qian H. Extraction and recycling utilization of metal ions (Cu^{2+}, Co^{2+} and Ni^{2+}) with magnetic polymer beads. Chem Eng J. 2012;200-202:104-112.
9. Senthil Kumar P, Senthamarai C, Sai Deepthi ASL, Bharani R. Adsorption isotherms, kinetics and mechanism of Pb(II) ions removal from aqueous solution using chemically modified agricultural waste. The Canadian Journal of Chemical Engineering. 2013;91(12):1950-1956.
10. Chen Y, He M, Wang C, Wei Y. A novel polyvinyltetrazole-grafted resin with high capacity for adsorption of Pb(ii), Cu(ii) and Cr(iii) ions from aqueous solutions. Journal of Materials Chemistry A. 2014;2(27):10444.
11. Cegłowski M, Schroeder G. Preparation of porous resin with Schiff base chelating groups for removal of heavy metal ions from aqueous solutions. Chem Eng J. 2015;263:402-411.
12. Suganya S, Saravanan A, Senthil Kumar P, Yashwanthraj M, Sundar Rajan P, Kayalvizhi K. Sequestration of Pb(II) and Ni(II) ions from aqueous solution using microalga Rhizoclonium hookeri: adsorption thermodynamics, kinetics, and equilibrium studies. Journal of Water Reuse and Desalination. 2016;7(2):214-227.
13. Liu P, Pu QS, Sun QY, Su ZX. Synthesis of rhodanine-bonded silica gel and its application in the preconcentration and separation of noble metals. Fresenius J Anal Chem. 2000;366(8):816-820.
14. Khan S, Kazi TG, Soylak M. Rapid ionic liquid-based ultrasound assisted dual magnetic microextraction to preconcentrate and separate cadmium-4-(2-thiazolylazo)-resorcinol complex from environmental and biological samples. Spectrochimica Acta Part A: Molecular and Biomolecular Spectroscopy. 2014;123:194-199.
15. Kang T, Li F, Baik S, Shao W, Ling D, Hyeon T. Surface design of magnetic nanoparticles for stimuli-responsive cancer imaging and therapy. Biomaterials. 2017;136:98-114.
16. Nasrollahzadeh M, Issaabadi Z, Varma RS. Magnetic Lignosulfonate-Supported Pd Complex: Renewable Resource-Derived Catalyst for Aqueous Suzuki–Miyaura Reaction. ACS Omega. 2019;4(10):14234-14241.
17. Rahimi L, Mansoori Y, Nuri A, Koohi-Zargar B, Esquivel D. A new Pd(II)-supported catalyst on magnetic SBA-15 for C C bond formation via the Heck and Hiyama cross-coupling reactions. Appl Organomet Chem. 2020;35(2).
18. Mousavi S, Mansoori Y, Nuri A, Koohi-Zargar B. A New Nitrogen Pd(II) Complex Immobilized on Magnetic Mesoporous Silica: A Retrievable Catalyst for C–C Bond Formation. Catal Lett. 2020;151(7):1923-1936.
19. Pooresmaeil M, Namazi H. Chitosan coated Fe_3O_4@Cd-MOF microspheres as an effective adsorbent for the removal of the amoxicillin from aqueous solution. Int J Biol Macromol. 2021;191:108-117.
20. Dupont D, Brullot W, Bloemen M, Verbiest T, Binnemans K. Selective Uptake of Rare Earths from Aqueous Solutions by EDTA-Functionalized Magnetic and Nonmagnetic Nanoparticles. ACS Applied Materials & Interfaces. 2014;6(7):4980-4988.
21. Jainae K, Sukpirom N, Fuangswasdi S, Unob F. Adsorption of Hg(II) from aqueous solutions by thiol-functionalized polymer-coated magnetic particles. Journal of Industrial and Engineering Chemistry. 2015;23:273-278.
22. Qiu X, Li N, Yang S, Chen D, Xu Q, Li H, et al. A new magnetic nanocomposite for selective detection and removal of trace copper ions from water. Journal of Materials Chemistry A. 2015;3(3):1265-1271.
23. Chen R, Cheng Y, Wang P, Wang Q, Wan S, Huang S, et al. Enhanced removal of Co(II) and Ni(II) from high-salinity aqueous solution using reductive self-assembly of three-dimensional magnetic fungal hyphal/graphene oxide nanofibers. Sci Total Environ. 2021;756:143871.
24. Wang Y, Zhang H, Yaseen M, Tong Z, Chen N, Shi H. Carboxymethylcellulose-chitosan film modified magnetic alkaline Ca-bentonite for the efficient removal of Pb(II) and Cd(II) from aqueous solution. Environmental Science and Pollution Research. 2021;28(23):30312-30322.
25. Bhatti RS, Shah S, Suresh, Krishan P, Sandhu JS. Recent Pharmacological Developments on Rhodanines and 2,4-Thiazolidinediones. International Journal of Medicinal Chemistry. 2013;2013:1-16.
26. Singh SJ, Chauhan SMS. Potassium carbonate catalyzed one pot four-component synthesis of rhodanine derivatives. Tetrahedron Lett. 2013;54(20):2484-2488.
27. Song J, Oh H, Kong H, Jang J. Polyrhodanine modified anodic aluminum oxide membrane for heavy metal ions removal. J

Hazard Mater. 2011;187(1-3):311-317.
28. Lee C-H, Chiang C-L, Liu S-J. Electrospun nanofibrous rhodanine/polymethylmethacrylate membranes for the removal of heavy metal ions. Sep Purif Technol. 2013;118:737-743.
29. Amiri A, Ghorbani M, Jahangiri M. A novel chitosan/polyrhodanine nanocomposite: preparation, characterisation and application for Ni(II) ions removal from aqueous solution. J Exp Nanosci. 2015;10(18):1374-1386.
30. Chen Y, Han S, Yang S, Pu Q. Rhodanine stabilized gold nanoparticles for sensitive and selective detection of mercury (II). Dyes and Pigments. 2017;142:126-131.
31. Rahmaninia A, Mansoori Y, Nasiri F. Surface-initiated atom transfer radical polymerization of a new rhodanine-based monomer for rapid magnetic removal of Co(II) ions from aqueous solutions. Polym Adv Technol. 2018;29(7):1988-2001.
32. Brown FC. 4-Thiazolidinones. Chem Rev. 1961;61(5):463-521.
33. Nagase H. Studies on Fungicides. XXI. Reaction of Dimethyl Acetylenedicarboxylate with Thioureas. Chemical and Pharmaceutical Bulletin. 1973;21(2):270-278.
34. Nasiri F, Zolali A, Kadkhoda J. Stereoselective Solvent-Free Synthesis of 4-Hydroxy-1,3-thiazinane-2-thiones. J Heterocycl Chem. 2015;53(3):937-940.
35. Baryshnikov GV, Minaev BF, Minaeva VA, Ågren H. Theoretical study of the conformational structure and thermodynamic properties of 5-(4-oxo-1,3-thiazolidine-2-ylidene)-rhodanine and ethyl-5-(4-oxo-1,3-thiazolidine-2-ylidene)-rhodanine-3-acetic acid as acceptor groups of indoline dyes. J Struct Chem. 2010;51(5):817-823.
36. Iijima K, Le Gal Y, Higashino T, Lorcy D, Mori T. Birhodanines and their sulfur analogues for air-stable n-channel organic transistors. Journal of Materials Chemistry C. 2017;5(35):9121-9127.
37. Rezaei M, Azizi K, Amani K. Copper–birhodanine complex immobilized on Fe_3O_4 nanoparticles: DFT studies and heterogeneous catalytic applications in the synthesis of propargylamines in aqueous medium. Appl Organomet Chem. 2017;32(3).
38. Nasiri F, Mansoori Y, Rostamzadeh N. Novel polyesters and polyester/Cloisite 30B nanocomposites based on a new rhodanine-based monomer. Polymer Science, Series B. 2017;59(3):268-280.
39. Nasiri F, Zolali A, Asadbegi S. Solvent-free One-pot Synthesis of 2,2′-dithioxo-[5,5′]bithiazolidinylidene-4,4′-diones. J Heterocycl Chem. 2015;53(3):989-992.
40. Nasiri F, Nazari P. One-pot solvent-free three-component reaction between primary amines, carbon disulfide, and 5-alkylidene rhodanines: a convenient synthesis of asymmetric birhodanines. Mol Divers. 2018;22(3):601-608.
41. Mirzaeinejad M, Mansoori Y, Amiri M. Amino functionalized ATRP-prepared polyacrylamide-g-magnetite nanoparticles for the effective removal of Cu(II) ions: Kinetics investigations. Materials Chemistry and Physics. 2018;205:195-205.
42. Theamdee P, Traiphol R, Rutnakornpituk B, Wichai U, Rutnakornpituk M. Surface modification of magnetite nanoparticle with azobenzene-containing water dispersible polymer. J Nanopart Res. 2011;13(10):4463-4477.
43. Bazargan A, Shek T-H, Hui C-W, McKay G. Optimising batch adsorbers for the removal of zinc from effluents using a sodium diimidoacetate ion exchange resin. Adsorption. 2017;23(4):477-489.
44. Ferreira GR, Segura T, de Souza FG, Umpierre AP, Machado F. Synthesis of poly(vinyl acetate)-based magnetic polymer microparticles. Eur Polym J. 2012;48(12):2050-2069.
45. Shull RD. Nanocrystalline and Nanocomposite Magnetic Materials and Their Applications. Journal of Iron and Steel Research International. 2007;14(4):69-74.
46. Hanawalt JD, Rinn HW, Frevel LK. Chemical Analysis by X-Ray Diffraction. Industrial & Engineering Chemistry Analytical Edition. 1938;10(9):457-512.
47. Choubey J, Bajpai AK. Investigation on magnetically controlled delivery of doxorubicin from superparamagnetic nanocarriers of gelatin crosslinked with genipin. J Mater Sci Mater Med. 2010;21(5):1573-1586.
48. Basavaraja C, Jo EA, Huh DS. Characterization and magnetic properties of conducting poly(N-vinylcarbazole)-capped magnetite nanocomposite Langmuir–Schaefer films. Mater Lett. 2010;64(6):762-764.
49. Playá N, Macías A, Ma Varela J, Sánchez A, Casas JS, Sordo J. Mono-organomercury and diorganothallium derivatives of rhodanine: Crystal structure of dimethyl(rhodaninato) thallium(III). Polyhedron. 1991;10(13):1465-1472.
50. Saxena A, Upadhyay R. Chemistry of the Thiazolidinone alone or along with Thiourea substituted Amine Complexes of Zinc (II). Oriental Journal Of Chemistry. 2012;28(1):599-601.
51. Mittal H, Ballav N, Mishra SB. Gum ghatti and Fe_3O_4 magnetic nanoparticles based nanocomposites for the effective adsorption of methylene blue from aqueous solution. Journal of Industrial and Engineering Chemistry. 2014;20(4):2184-2192.
52. Badruddoza AZM, Hazel GSS, Hidajat K, Uddin MS. Synthesis of carboxymethyl-β-cyclodextrin conjugated magnetic nano-adsorbent for removal of methylene blue. Colloids Surf Physicochem Eng Aspects. 2010;367(1-3):85-95.
53. Teker M, Saltabaş Ö, İmamoğlu M. Adsorption of cobalt by activated carbon from the rice hulls. Journal of Environmental Science and Health Part A: Environmental Science and Engineering and Toxicology. 1997;32(8):2077-2086.
54. Ebner AD, Ritter JA, Navratil JD. Adsorption of Cesium, Strontium, and Cobalt Ions on Magnetite and a Magnetite–Silica Composite. Industrial and Engineering Chemistry Research. 2001;40(7):1615-1623.
55. Yavuz Ö, Altunkaynak Y, Güzel F. Removal of copper, nickel, cobalt and manganese from aqueous solution by kaolinite. Water Res. 2003;37(4):948-952.
56. Sulaymon AH, Abid BA, Al-Najar JA. Removal of lead copper chromium and cobalt ions onto granular activated carbon in batch and fixed-bed adsorbers. Chem Eng J. 2009;155(3):647-653.
57. He M, Zhu Y, Yang Y, Han B, Zhang Y. Adsorption of cobalt(II) ions from aqueous solutions by palygorskite. Applied Clay Science. 2011;54(3-4):292-296.
58. Wang Q, Li J, Chen C, Ren X, Hu J, Wang X. Removal of cobalt from aqueous solution by magnetic multiwalled carbon nanotube/iron oxide composites. Chem Eng J. 2011;174(1):126-133.
59. Padala AN, Bhaskarapillai A, Velmurugan S, Narasimhan SV. Sorption behaviour of Co(II) and Cu(II) on chitosan in presence of nitrilotriacetic acid. J Hazard Mater. 2011;191(1-3):110-117.
60. Chen Y, Wang J. The characteristics and mechanism of Co(II) removal from aqueous solution by a novel xanthate-modified magnetic chitosan. Nucl Eng Des. 2012;242:452-457.
61. Diniz KM, Gorla FA, Ribeiro ES, Nascimento MBOd, Corrêa RJ, Tarley CRT, et al. Preparation of $SiO_2/Nb_2O_5/ZnO$ mixed oxide by sol–gel method and its application for adsorption studies and on-line preconcentration of cobalt ions from aqueous medium. Chem Eng J. 2014;239:233-241.
62. Alakhras F, Al-Shahrani H, Al-Abbad E, Al-Rimawi F, Ouerfelli N. Removal of Pb(II) Metal Ions from Aqueous Solutions Using Chitosan-Vanillin Derivatives of Chelating Polymers. Polish Journal of Environmental Studies. 2019;28(3):1523-1534.